

Inhibitors of the Elastase LasB for the treatment of *Pseudomonas aeruginosa* lung infections

5 **Authors:** Jelena Konstantinović^{1,§}, Andreas M. Kany^{1,‡}, Alaa Alhayek^{1,‡}, Ahmed S. Abdelsamie^{1,2},
Asfandyar Sikandar¹, Katrin Voos^{3,‡}, Yiwen Yao⁴, Anastasia Andreas¹, Roya Shafiei^{1,5}, Brigitta
Loretz¹, Esther Schönauer⁶, Robert Bals^{1,4}, Hans Brandstetter⁶, Rolf W. Hartmann^{1,5}, Christian
Ducho³, Claus-Michael Lehr^{1,5}, Christoph Beisswenger⁴, Rolf Müller^{1,5,7}, Katharina Rox⁸, Jörg
Haupenthal¹, Anna K.H. Hirsch^{1,5,7*}

Affiliations:

10 ¹Helmholtz Institute for Pharmaceutical Research Saarland, (HIPS)–Helmholtz Centre for
Infection Research (HZI); Saarbrücken, 66123, Germany.

²Department of Chemistry of Natural and Microbial Products, Institute of Pharmaceutical and
Drug Industries Research, National Research Centre, El-Buhouth St., Dokki, Cairo, 12622,
Egypt

15 ³Department of Pharmacy, Pharmaceutical and Medicinal Chemistry, Saarland University;
Saarbrücken, 66123, Germany.

⁴Department of Internal Medicine V – Pulmonology, Allergology and Critical Care
Medicine, Saarland University; Homburg, 66421, Germany.

⁵Department of Pharmacy, Saarland University; Saarbrücken, 66123, Germany.

20 ⁶Department of Biosciences and Medical Biology, Division of Structural Biology, University
of Salzburg; Salzburg, 5020, Austria.

⁷Helmholtz International lab for Anti-infectives, Saarbrücken, 66123, Germany

⁸Department of Chemical Biology (CBIO), Helmholtz Centre for Infection Research (HZI);
Braunschweig, 38124, Germany.

25 *Corresponding author. Email: anna.hirsch@helmholtz-hips.de

‡These authors contributed equally

Present addresses:

30 §Innovation Campus Berlin (Nuvisan ICB GmbH); Berlin, 13353, Germany; ‡ Merck
KGaA; Darmstadt, 64293, Germany

Abstract

Infections caused by the Gram-negative pathogen *Pseudomonas aeruginosa* are emerging worldwide as a major threat to human health. Conventional antibiotic monotherapy suffers from rapid resistance development, underlining urgent need for novel treatment concepts. Here, we report on a non-traditional approach to combat *P. aeruginosa*-derived infections by targeting its main virulence factor, the elastase LasB. We discovered a new chemical class of phosphonates with an outstanding in vitro ADMET and PK profile, auspicious activity both in vitro and in vivo. We established the mode of action through a co-crystal structure of our lead compound with LasB and in several in vitro and ex vivo models. The proof of concept of a combination of our pathoblocker with levofloxacin in a murine neutropenic lung infection model and the reduction of LasB protein levels in blood as a proof of target engagement demonstrate the great potential for use as an adjunctive treatment of lung infections in humans.

Introduction

The silent pandemic of antimicrobial resistance is a global health threat, affecting millions of people worldwide. It is caused by natural mechanisms of pathogen defense, over- as well as misuse of antibiotics in humans as well as in animal husbandry. Consequently, even common infections are becoming increasingly problematic to treat. This leads to augmented costs in the healthcare sector including the necessity for longer treatments, and, despite that, still high mortality rates^{1,2,3,4}. *Pseudomonas aeruginosa* is a Gram-negative bacterium which typically infects lungs, the urinary tract and wounds, leading to severe infections challenging to treat due to drug-resistance⁵. In 2017, the World Health Organization (WHO) published a priority list of pathogens raising the topic of an urgent need for novel antibiotics, in particular *P. aeruginosa*, identified as a top-three critical pathogen devoid of sufficient treatment options for drug-resistant strains⁶. *P. aeruginosa* is one of the major pathogens in cystic fibrosis (CF), as well as in non-cystic fibrosis bronchiectasis (NCFB) patients, leading to chronic lung infection and poor pulmonary function^{7,8}. Furthermore, the pathogen plays important roles in hospital-acquired and ventilator-associated pneumonia^{9,10}, urinary-tract infections¹¹, keratitis¹² and wound infections¹³. Taken together, there is an immediate necessity for the development of new anti-infectives – antibiotics with novel mechanisms of action or non-traditional approaches to fight antibiotic resistance; in particular, against Gram-negative pathogens¹⁴.

Recently, significant efforts have been put into the development of ‘pathoblockers’ – agents capable of blocking bacterial virulence by disarming, rather than killing the pathogen. This should reduce the selection pressure and the formation of resistance^{15,16}. In particular, pathoblocker-antibiotic combinations are expected to have a synergistic effect and result in a more successful treatment¹⁷. *P. aeruginosa* secretes several virulence factors that serve as promising targets for the development of such pathoblockers¹⁸. A central contributor to *P. aeruginosa* virulence is the elastase LasB, which plays a crucial role in the infection process. This extracellular proteolytic enzyme is responsible for tissue damage and has a destructive effect on various components of the immune system¹⁹. These pathological roles strongly advise the development of drugs against *P. aeruginosa* by inactivating LasB, as recently thoroughly reviewed by Everett and Davies²⁰. In addition, one recent study came to the remarkable conclusion that elastase activity appears to be associated with 30-day mortality in intensive care unit patients²¹. LasB or pseudolysin is a zinc-dependent metalloenzyme with an additional metal cation (Ca²⁺) as a cofactor in the active site²². Therefore, the vast majority of the studied inhibitors contain zinc-binding groups (ZBGs), such as thiols^{23,24}, hydroxamates²⁵, carboxylic acids²⁶, tropolones²⁷ or 3-hydroxypyridine-4(1*H*)-thiones²⁸.

We have extensively explored these ZBGs in the past few years and used those findings as the basis for the current work^{29,30,31,32,33}.

Given the instability of thiols due to oxidation, we here present a systematic study of the 15 most common ZBGs as a suitable replacement for the thiol liability present in our inhibitors of LasB. Our ultimate goal is the identification of a stable, active and safe pathoblocker to fill the dry antibiotic pipeline. In view of the envisioned application of these compounds as novel anti-infectives in vivo, the rationale of the most favorable ZBG was supported by in vitro absorption, distribution, metabolism, excretion and toxicity (ADMET) profiling. Taken together, these data strongly favored the phosphonic acid derivatives as the most promising class. Pharmacokinetic studies in mice showed that these compounds have an excellent retention in lung tissue and epithelial lining fluid (ELF). In a pharmacodynamics study, the combination of the phosphonic acid inhibitor **4b** with levofloxacin reduced the bacterial burden below stasis in mice infected with *P. aeruginosa* DSM-1117. Additionally, a reduction of LasB protein in blood was observed demonstrating target attainment of our pathoblockers.

Results and Discussion

Replacing the thiol

Previously, we reported on *N*-aryl-2-isobutylmercaptoacetamides showing sub-micromolar potencies against *P. aeruginosa* elastase LasB²⁹. The approach to inhibit LasB (as a metalloprotease) comes with the intrinsic challenge of target selectivity over biochemically related human off-targets such as the human matrix-metalloproteases (MMPs). Despite being highly potent and selective over MMPs, the potential therapeutic application of *N*-aryl-2-isobutylmercaptoacetamides is limited due to the poor chemical stability of the free thiol group. Recently, we performed a screening of various ZBGs and investigated their effect on the activity against ColH, a collagenase secreted by *Clostridium histolyticum*, a target that is structurally and mechanistically closely related to LasB³⁴. Phosphonate derivative **1** demonstrated modest activity towards LasB (Fig. 1). Our recent work on *N*-aryl-2-isobutylmercaptoacetamide **2**²⁹ suggested the importance of an alpha-alkyl substituent for the inhibition of LasB. Therefore, we designed 15 derivatives bearing an alpha-isobutyl side chain and different ZBGs, which yielded sulfonates, triazoles, hydroxamates and phosphonates as possible alternatives to the thiol. Among them, the most potent turned out to be the hydroxamic acid derivative **3g** and the phosphonic acid **4a**. Subsequent exploration of their in vitro ADMET properties confirmed phosphonates to be the most promising class. The detailed synthetic procedures of mentioned inhibitors have been described in Supplementary information (Fig. S1–S5).

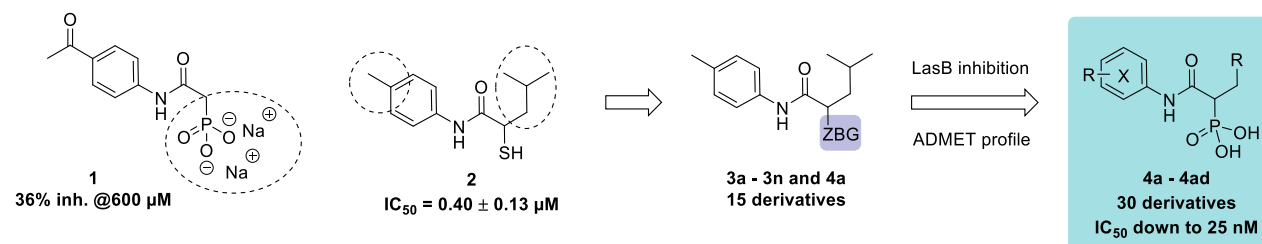


Fig. 1. Optimization of **1** leading to phosphonate derivatives with nanomolar IC_{50} values against LasB

LasB inhibition by compounds with different ZBGs

We evaluated new derivatives for in vitro inhibition of LasB (Table S2) using a functional FRET-based assay, as established by Nishino et al³⁵. The corresponding thiol analogue **2** was used as comparator²⁹. Among 15 derivatives, five compounds showed IC₅₀ values below 20 μM. The sulfonic acid derivative **3i** and two triazole derivatives **3l** and **3m** showed activity in the μM range, while the most pronounced activity was observed for the hydroxamic acid **3g** (IC₅₀ = 14 ± 1 nM) and the phosphonic acid derivative **4a** (IC₅₀ = 51 ± 7 nM). We improved activity by 30-fold and 8-fold, respectively, compared to our previous thiol hit **2**. As it has been shown previously that surfactant can impair the activity of drugs targeting the lung³⁶, we determined IC₅₀ values in presence of 1% pulmonary surfactant for our frontrunners. **4b** did only exhibit a 3-fold increase in IC₅₀, resulting in potency in the nanomolar range (IC₅₀ = 76 ± 23 nM). A detailed discussion on the structure–activity relationships (SAR) of phosphonic acid derivatives is provided in the Supplementary information (Table S3–S4).

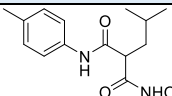
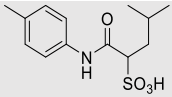
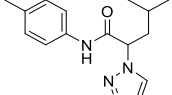
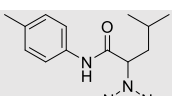
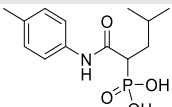
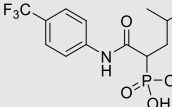
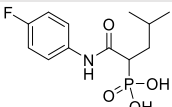
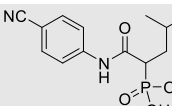
ADMET profiling

To select the most suitable ZBG for our LasB inhibitors, we considered their in vitro ADMET profile along with their in vitro potency (Table 1). For this purpose, we compared hydroxamic acid derivative **3g**, sulfonic acid **3i** and the two triazoles **3l** and **3m**, with the phosphonic acids **4a**, **4b**, **4h** and **4k**. A key decision criterion was permeability across Calu-3 monolayers, which constitutes an important feature of anti-pseudomonal drugs targeting the lung. Since our overall goal was to achieve good lung retention after pulmonary administration, low permeability was desirable to avoid rapid dissemination of the LasB inhibitor into systemic circulation. Sulfonic acid **3i** (P_{app} = 0.47 × 10⁻⁶ cm/s) and phosphonic acids **4a** and **4b** (P_{app} = 0.97 × 10⁻⁶ cm/s and 2.8 × 10⁻⁶ cm/s, respectively) showed the lowest P_{app} values. Additionally, we investigated kinetic solubility and lipophilicity (logD_{7.4}), murine and human metabolic stability, as well as murine plasma stability (Table 1). The results suggest that the phosphonic acid derivatives have the best overall ADMET profile, i.e. high solubility, low lung permeability and high stability in mouse and human liver S9 fractions and mouse plasma. Further, we profiled three selected phosphonates regarding their metabolism in different species, confirming excellent metabolic and plasma stability in rat and minipig (Table S5).

To rationalize the observed striking differences in cell permeability, we correlated the measured permeabilities P_{app} with chromatographic lipophilicities logD_{7.4} (Fig. S6). Notably, there is a very good correlation between compound lipophilicity and Calu-3 permeability for our set of LasB inhibitors (R² = 0.9865). Namely, hydroxamate **3g** as well as triazoles **3l** and **3m** give significantly higher logD_{7.4} values (>1.8) compared to the phosphonates (logD_{7.4} ≤ 0). This correlation strengthens our selection of phosphonates as the most promising ZBG, given that their high hydrophilicity and negative charge at physiological pH reduces the permeability across the more lipophilic cell layer, hence favoring lung retention. Furthermore, this good correlation can potentially be applied in the future as a useful tool to rationally design compounds with physicochemical properties favorable for good lung exposure.

Representative derivatives were tested for their cytotoxicity on three human cell-lines – HepG2 (hepatocellular carcinoma), HEK293 (embryonal kidney) and A549 (lung carcinoma). All measured growth inhibition values were less than 30% at 100 μM, thus, all compounds showed an excellent profile and did not bear cytotoxicity potential at concentrations relevant for in vivo assessment (Table 1, Table S6).

Table 1. LasB inhibition and absorption, distribution, metabolism, excretion, and toxicity (ADMET) profiling of selected compounds bearing different zinc-binding groups (ZBGs)

| Compound | Class | LasB IC ₅₀ (nM) | logD _{7.4} | S9 Cl _{int} [μL/mg/min] | | Plasma | Calu-3 | % growth inhibition of A549 cells ^a |
|----------|---|-------------------------------|---------------------|----------------------------------|------------|---------------------------------|--|--|
| | | | | Mouse | Human | T _{1/2} [min] Mouse | permeability P _{app} [10 ⁻⁶ cm/s] | |
| 3g |  | 14 ± 1 | 1.81 | 64 ± 10 | <5.8 | >150 | 9.8 ± 2.6 | 11 ± 9 |
| 3i |  | 16 ± 0 μM | -0.64 | <5.8 | <5.8 | >150 | 0.47 ± 0.36 | n.i. |
| 3l |  | 2.8 ± 0.1 μM | 2.87 | 90 ± 9 | 8.8 ± 1.2 | >150 | 17 ± 1 | n.i. |
| 3m |  | 5.3 ± 0.2 μM | 3.50 | 356 ± 45 | 18.5 ± 0.9 | >150 | 18 ± 1 | n.i. |
| 4a |  | 51 ± 7 | -0.64 | <5.8 | <5.8 | >150 | 0.97 ± 0.21 | n.i. |
| 4b |  | 26 ± 8 | 0.00 | <5.8 | <5.8 | >150 | 2.8 ± 1.2 | n.i. |
| 4h |  | 93 ± 22 | -0.79 | <5.8 | <5.8 | >150 | n.d. | n.d. |
| 4k |  | 25 ± 1 | -0.87 | <5.8 | <5.8 | >150 | n.d. | n.i. |

^aAfter 48 h at 100 μM; n.d. = not determined; n.i. = <10 % inhibition; kinetic solubility was determined to be >200 μM for all tested compounds

5

Biological evaluation of phosphonic acids in target validation models

To assess the activity of the phosphonic acid class in target-validation models, we tested selected compounds in two different cell-based assays including lung organoids, constituting an increasingly complex matrix close to the physiological setting, as well as in a simple in vivo model based on *G. mellonella* larvae.

10

Evaluation of LasB inhibitors in A549 cells treated with *P. aeruginosa* PAO1 and PA14 supernatants

First, we challenged the human lung adenocarcinoma cell line A549 with culture supernatants (csn) derived from wild-type *P. aeruginosa* PAO1 or PA14 (wt PAO1; wt PA14) as well as *lasB* knockout strains (PAO1 $\Delta lasB$; PA14 $\Delta lasB$) to assess the inhibitory effect of two phosphonate LasB inhibitors, **4a** and **4b**, on the proteolytic and elastolytic and cytotoxic properties. Both compounds demonstrated an excellent dose-dependent reduction of LasB-related cytotoxicity in csn-treated cells, comparable to the levels of the knockout strain. This illustrates impressively the relevance of LasB and its inhibition (Fig. S7A–B). Interestingly, higher concentrations of **4b** were necessary to achieve similar effects against PA14 csn, which could be attributed to the higher amounts of secreted LasB by PA14 (Fig. S7 D).

Compound **4b** sustained viability of cells, even at low concentrations (Fig. 2A, Fig. S8)^{29,32,37}. LasB targets the extracellular matrix component collagen and leads to its degradation. **4b** reduced cleavage of collagen by 20% at a concentration of 3.15 μM (Fig. S7 C)^{20,38,39}. To exclude that effects of **4b** might be attributed to other proteases in PA14 csn, we deployed PA14 $\Delta lasB$ csn. No effect on the viability and on collagen was observed using the $\Delta lasB$ (Fig. S7 B–C). This demonstrates that **4b** selectively inhibited LasB and did not affect other proteases in the csn.

Lung organoid assay

In the past years, lung organoids have been extensively used to study pulmonary diseases due to the high resemblance of their structural features and their functions with the native lung^{40,41}. We studied the effect of PA14 csn on the viability of 3D lung organoids and the rescue effect by inhibitors **4a** and **4b** (Fig. S9). In this experiment, primary human bronchial epithelial cells (HBECs) were differentiated to human 3D bronchospheres⁴² and challenged with 5% PA14 csn. LasB inhibitors **4a** and **4b** did not have significant toxic effects on the non-treated lung organoids in concentrations tested up to 100 μM . Upon treatment with PA14 csn, viability of the organoids was reduced to 30–60%. By contrast, treatment with LasB inhibitors **4a** and **4b** resulted in a strong beneficial effect as viability of the organoids was improved in a dose-dependent manner (Fig. S9). Therefore, effectiveness of LasB inhibitors was also demonstrated in the 3D model constituting a complex matrix system close to the physiological situation.

Effect of **4b** in a *Galleria mellonella* infection model

Next, we infected *G. mellonella* larvae, a standard model for evaluation of novel anti-infectives⁴³, with wt PA14 and treated them with **4b** and tobramycin (individually and in combination), a standard-of-care antibiotic in CF⁴⁴. For the combination experiments, we chose a lower tobramycin dose (10.7 nmol, corresponding to 0.5 $\mu\text{g}/\text{mL}$ in the dosed solution), aiming at the improvement of a sub-efficacious dose of tobramycin with **4b**. A higher tobramycin dose of 17 nmol (0.8 $\mu\text{g}/\text{mL}$) was used as 100% efficacious dose of the antibiotic. While treatment with **4b** or tobramycin at a low dose alone only led to a slight increase in survival (25% and 5%, respectively), the combination of **4b** and tobramycin significantly improved the survival by 40% (Fig. 2B).

Importantly, **4b** as well as further selected phosphonates do not possess any antibacterial activity up to 100 μM (Fig. S10 C). In line with this, the combination with tobramycin did not increase the antibacterial activity of the antibiotic alone in vitro (Fig. S10 A-B), indicating that the observed improvement of in vivo activity was caused by the antivirulence effect of the LasB inhibitor. Hence, this study reinforced the potential of our compound to boost the efficacy of antibiotics in vivo by targeting the virulence factor LasB.

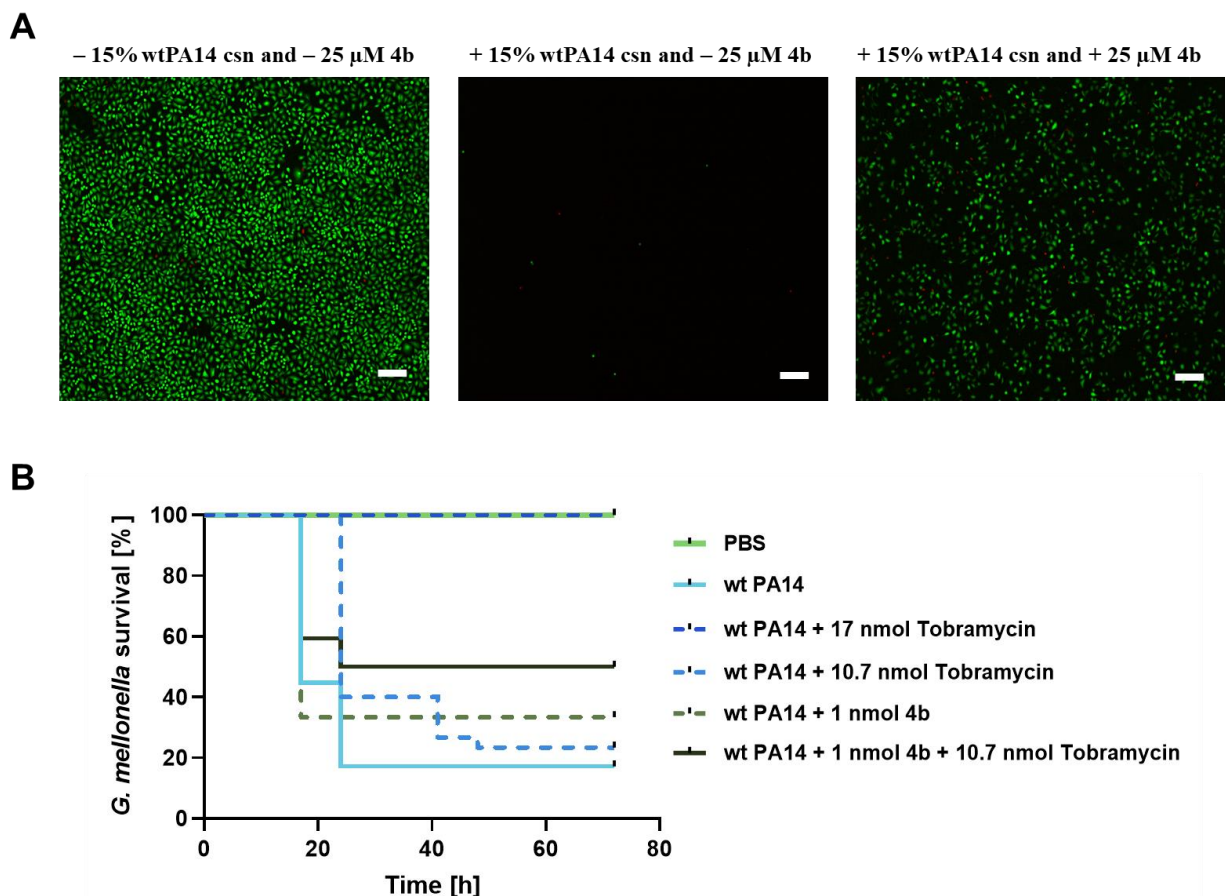


Fig. 2. (A) **4b** maintained the viability of lung (A549) cells upon treatment with 15% wt PA14 csn. Live/dead imaging with A549 cells challenged with 15% (*v/v*) of PA14 csn with and without **4b**. Green signals: living cells and red signals: dead cells, red signals in some cases were lost because the detached cells were washed away after the rinsing step with PBS. Scale bar: 200 μ m for images. (B) Probability of survival of the *Galleria mellonella* larvae infected with wt PA14: The survival of larvae infected with wt PA14 is shown after treatment with 1 nmol **4b**, 10.7 nmol tobramycin or a combination of both. The survival in the PBS-**4b** or Tobramycin or combination of both treated groups was 100%. The statistical difference between groups treated with 1 nmol **4b** + 10.7 nmol tobramycin and treated with only wt PA14 is $p = 0.0005$ (log-rank). Each curve represents results of three independent experiments. wt PA14: wild-type PA14, Δ PA14: LasB knockout PA14, csn: culture supernatant.

Selectivity for LasB over human off-targets and other bacterial proteases as well as advanced off-target safety screening and zebrafish embryo toxicity

Next, we aimed to test selectivity against human off-targets and other bacterial proteases and safety. We assessed four most potent inhibitors (**4a**, **4b**, **4k** and **4l**) which showed a significantly improved selectivity profile against human off-targets compared to our previously published hit, compound **2** (Table S7). **4b** and **4k** had slight effects at 100 μ M against MMP-1, -2 and -3, which was negligible when compared to their activity towards LasB ($IC_{50} \sim 25$ nM). On the contrary, the hydroxamic acid **3g**, although being 2-fold more potent compared to the best phosphonate inhibitor, exhibited slight effects on MMP-1, -2 and -3 and inhibition of tumor necrosis factor- α converting enzyme (TACE) in the micromolar range (Table S7). We previously reported on

a structural similarity between inhibitors of *P. aeruginosa* elastase LasB and *C. histolyticum* collagenase ColH^{30,33,34}. Most of our newly developed inhibitors demonstrated no or only weak inhibition of ColH-PD (**4a**, **4b**, **4c**, **4d**, **4f**), with the notable exception of **4g**. This compound was a more potent ColH inhibitor than the previous 'best-in-class' phosphonate inhibitor of ColH, i.e., **1** (see Supplementary information). It might therefore be developed towards a dual inhibitor of both metalloprotease virulence factors LasB and ColH if a medical need for such an agent with dual activity arises (Table S8).

Then, we assessed potential additional safety liabilities of **4a** and **4b** using the Eurofins SafetyScreen44 panel to identify the most important off-target interactions at an early stage. When tested at a concentration of 10 μ M, compound **4a** demonstrated an excellent safety profile with no significant inhibition of any of the mentioned targets (Fig. S11). Furthermore, to gain a deeper insight into the potential clinical applicability, we investigated the toxicity of compounds *in vivo* on zebrafish embryos. Compounds **4a** and **4b** demonstrated a maximum tolerated concentration (MTC) of ≥ 100 μ M (Table S9). In summary, **4a** and **4b** demonstrated an excellent safety profile qualifying for additional *in vivo* preclinical testing.

Pharmacokinetic studies in mice

To further assess the potential of the new inhibitors for the treatment of lung infections, we subjected five selected compounds (**3g**, **3i**, **3l**, **4a** and **4b**) to pharmacokinetic studies in mice as a cassette dosing via intratracheal (IT) administration. The selection comprised representatives bearing different ZBGs in order to assess whether the observed differences in their *in vitro* permeabilities also resulted in different lung retentions *in vivo*. Hydroxamic acid **3g** and triazole derivative **3l** were found in ELF and lung tissue at significantly lower concentrations compared to sulfonic acid **3i** and phosphonic acids **4a** and **4b**. Moreover, hydroxamic acid **3g** was not detected 2 h after administration, which is perfectly in line with the observed differences in Calu-3 cell permeation. Quite remarkably, the concentrations of both phosphonic acids **4a** and **4b** were significantly above the IC₅₀ values determined in the FRET-assay in presence of surfactant (Fig. 3A+B, Table S10). The concentration levels of the five selected compounds in BALF, plasma, urine, kidney and liver tissue are summarized in the Supplementary information (Fig. S12).

Following IT cassette dosing, we performed a more focused PK study with compound **4b** at a single dose of 10 mg/kg, administered by nebulization (Fig. 3C). Selection of this compound for further *in vivo* analysis was based on the highest levels reached in ELF. Samples were analyzed for a period of 24 h. The compound rapidly appeared systemically and was detected in plasma, urine, ELF, lung tissue, kidney, and liver already after 15 min (Fig. 3B). Still, the compound had high initial ELF levels with a C_{max} of about 20 μ g/mL (~770-fold relative to the IC₅₀ value in presence of surfactant) and remaining in a moderate range until 24 h (Table S11). Lung tissue concentrations followed similar kinetics, although the concentration levels dropped significantly after 8 h. **4b** appeared rapidly in plasma with a T_{max} of about 4 h and a C_{max} of about 633 ng/mL (Fig. 3B, Table S12). Nevertheless, **4b** exhibited only a moderate to low fractionated plasma clearance (Table S12). Furthermore, low compound levels were observed in the liver tissue, whereas kidney tissue showed increasing levels. In line with the observed absence of liver metabolism *in vitro* and high concentrations found in urine, these findings suggest primarily renal clearance.

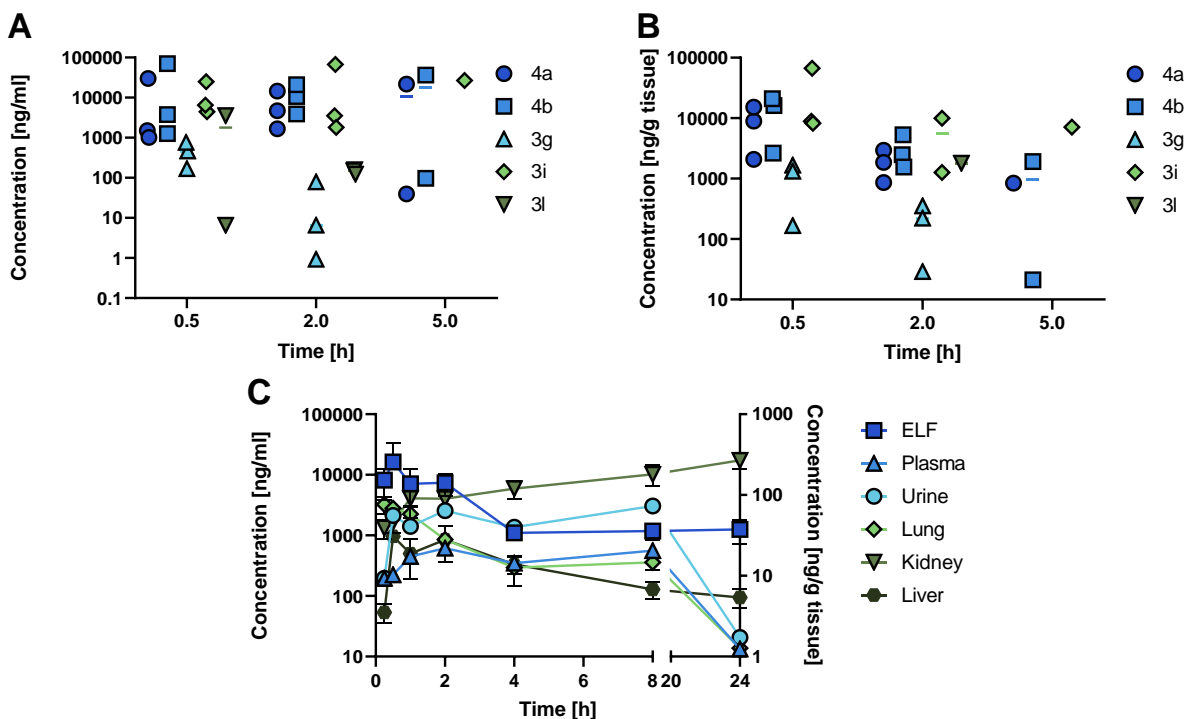


Fig. 3. (A) Concentrations of five selected ZBGs in ELF and (B) lung tissue after IT administration at 0.25 mg/kg (cassette dosing). (C) Concentrations of **4b** after nebulization of 10 mg/kg in ELF, plasma, urine, lung tissue, kidney tissue and liver tissue.

5

Pharmacodynamic studies in mice infected with *P. aeruginosa* DSM-1117

Encouraged by the results of **4b** in several in vitro and ex vivo assays, its efficacy in the in vivo infection model in *G. mellonella*, as well as the excellent lung and ELF retention after IT administration (0.25 mg/kg, cassette dosing) and nebulization (10 mg/kg), we performed a pharmacodynamic (PD) study using a neutropenic lung infection model with *P. aeruginosa* DSM-1117. In this experiment, we evaluated the effect of the antibiotic levofloxacin at 25 mg/kg, **4b** at 10 mg/kg TID, and a combination of both on the number of CFU in the lungs of the mice. The bacteria and **4b** were applied by nebulization, whereas levofloxacin was administered IP. Figure 4A shows the bacterial growth in lung tissue. A slight growth of bacteria was observed in the vehicle control group compared to the inoculum control. The levofloxacin group reduced the bacterial burden back to stasis, while **4b** alone did not show an effect on the number of CFU. Remarkably, the combination of **4b** and levofloxacin showed a clear synergistic effect, significantly reducing the bacterial burden below stasis. Moreover, assessment of LasB protein levels in blood as an indicator of dissemination showed a clear reduction for levofloxacin and the combination group compared to the vehicle group and back to the level of the inoculum control group. Remarkably, a strong reduction was also observed for the **4b** only group, although no effect on CFU had been detected in lung tissue. This reduction in presence of the LasB inhibitor, **4b**, and in absence of levofloxacin provided the proof of concept and target engagement (Fig. 4B).

10

15

20

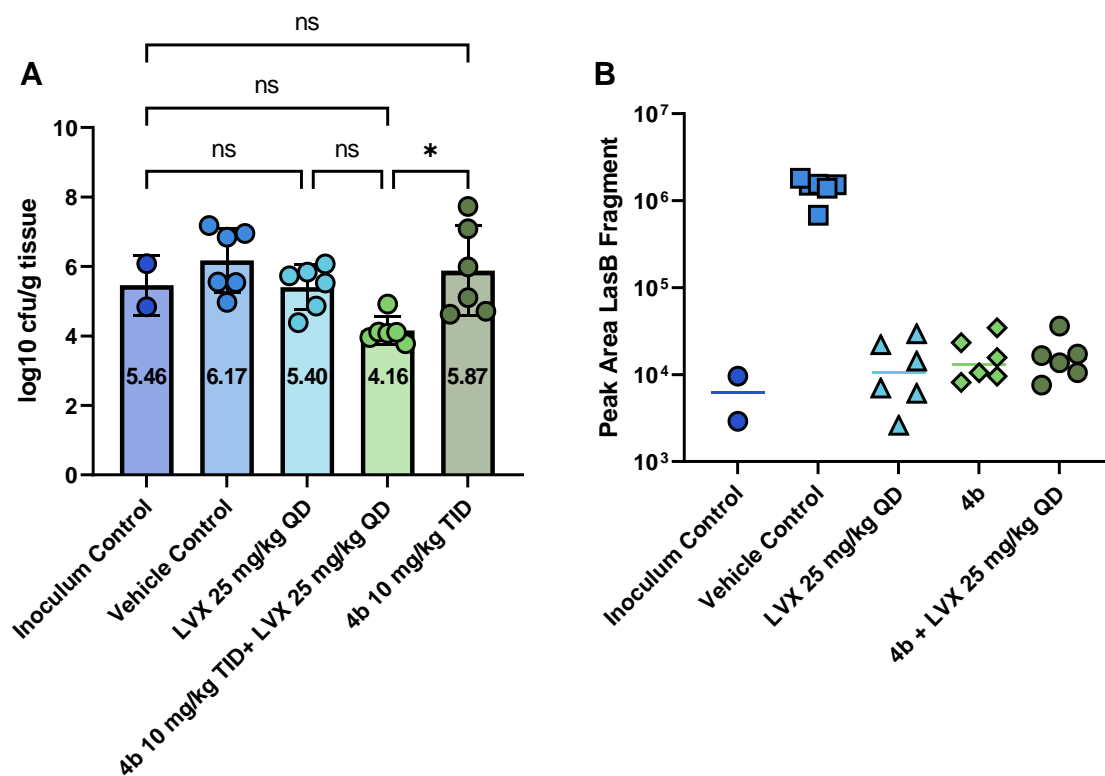


Figure 4. (A) Bacterial growth in lung tissue given as log₁₀ cfu/g tissue. Mice in all groups were treated with *P. aeruginosa* DSM-1117. Inoculum control – the number of colony-forming units (cfu) in the lungs was determined 15 min after infection; all other lungs were taken after 24 h; vehicle control – mice treated with a vehicle; LVX 25 mg/kg – mice treated with levofloxacin; **4b** 10 mg/kg TID (3 times per day) + LVX 25 mg/kg – mice treated with a combination of **4b** and levofloxacin; **4b** 10 mg/kg TID – mice treated with **4b**. (B) LasB levels in blood in mice infected with *P. aeruginosa* DSM-1117.

Crystal structure of **4b**

To elucidate the binding mode of phosphonic acid derivatives, we co-crystallized **4b** with LasB (Fig. 5A). Full details of the data collection and refinement statistics can be found in the Supplementary information (Table S13). The compound binds in a fashion that is similar to a previously reported α -substituted mercaptoacetamide derivative (PDB code: 7OC7)³¹ and occupies the S1'-S2' pockets with the phosphonate group coordinating the active site Zn²⁺ cation (Fig. S13A). In addition, **4b** also forms a number of additional H bonds and hydrophobic interactions that explain the significant improvement in activity over the mercaptoacetamide class (Fig. 5B). The carbonyl oxygen of **4b** forms a bidentate hydrogen bond with Arg198, while the side chains of His223, Glu141 and Asn112 form hydrogen bonds with the phosphonate and amide groups. The aryl group occupies the wide, open and solvent-accessible entrance of the lipophilic S2' binding pocket, which rationalizes the tolerance for substitution at this position (Fig. S13B). The replacement of the isobutyl group by bulkier substituents is detrimental likely due to the steric constraints of the S1' pocket that cannot accommodate such large groups without a steric clash (Fig. S13A).

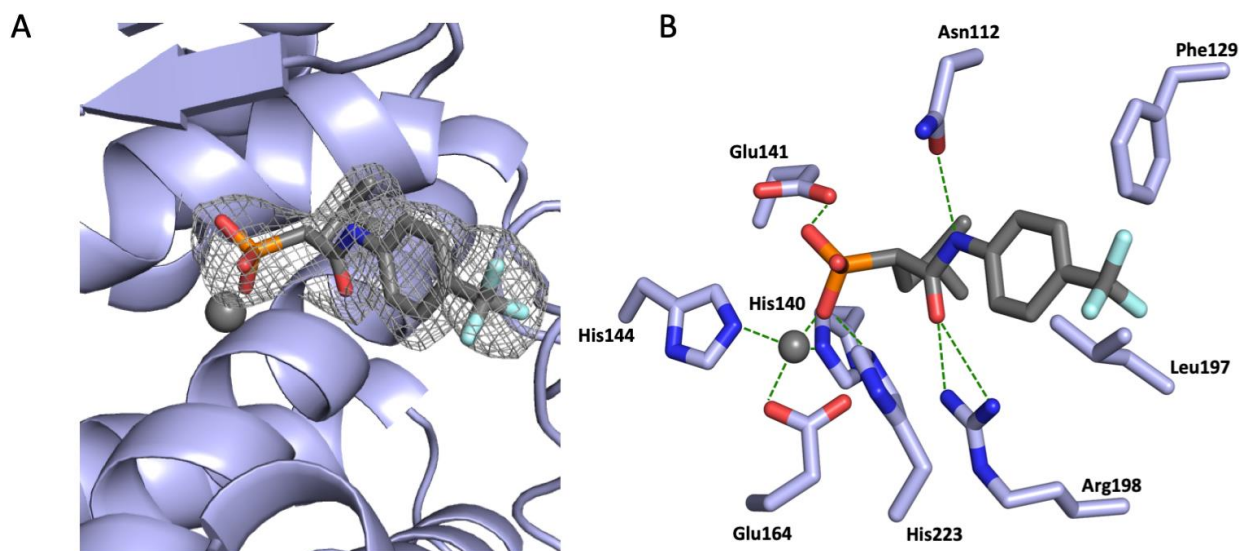


Fig. 5. Crystal structure of LasB in complex with **4b** (PDB code: 8CC4). (A) Cartoon representation of LasB (slate) in complex with **4b** (gray). The gray isomesh represents polder map of **4b** contoured at 3σ . (B) Schematic 2-D representation of LasB-**4b** interactions. Hydrogen bonds are displayed in dotted green lines, while all other residues exhibit hydrophobic interactions with the ligand.

Conclusion

A systematic exploration of ZBGs furnished a new class of phosphonic acid inhibitors showing nanomolar potency towards LasB and an excellent *in vitro* ADMET profile. We demonstrated that the compounds with the lowest permeability in the Calu-3 assay are at the same time showing the highest levels in ELF and a good lung retention with concentrations several magnitudes above IC_{50} values in presence of surfactant. This correlation of Calu-3 *in vitro* and PK *in vivo* data supports the use of Calu-3 assays as a predictive tool for the selection of compounds for *in vivo* studies, thereby increasing the success rate of these animal models while at the same time reducing the number of animals needed for testing. In the *G. mellonella* infection model, compound **4b** in combination with tobramycin demonstrated a significant improvement in survival which was translated into efficacy in a murine neutropenic lung infection model with *P. aeruginosa* DSM-1117, where the same compound in combination with levofloxacin reduced the bacterial burden significantly below stasis. Further *in vivo* proof of concept and target engagement was demonstrated by significantly reduced LasB levels in the blood even when **4b** was used as monotherapy. Without affecting bacterial growth while at the same time clearly demonstrating strong antivirulence effects against LasB *in vitro* and in several target-validation models, the potential of our inhibitors as a new class to be used in a combination therapy with standard-of-care antibiotics for the treatment of lung infections in humans is supported. In conclusion, our study provides novel pathoblockers targeting LasB with high potency, excellent safety and selectivity profile and demonstrated *in vivo* proof-of-concept as well as proof of target engagement, perfectly suited for further development via inhalative administration to enrich treatment options of infections in CF and NCFB patients⁴⁵.

Methods

Chemistry. All reagents were used from commercial suppliers without further purification. Procedures were not optimized regarding yield. NMR spectra were recorded on a Bruker AV 500 (500 MHz) spectrometer. Chemical shifts are given in parts per million (ppm) and referenced against the residual proton, ^1H , or carbon, ^{13}C , resonances of the >99% deuterated solvents as internal reference. Coupling constants (J) are given in Hertz. Data are reported as follows: chemical shift, multiplicity, coupling constants, and integration. Liquid chromatography-mass spectrometry was performed on a LC-MS system, consisting of a Dionex UltiMate 3000 pump, autosampler, column compartment and detector (Thermo Fisher Scientific, Dreieich, Germany) and ESI quadrupole MS (MSQ Plus or ISQ EC, Thermo Fisher Scientific, Dreieich, Germany). High resolution mass was determined by LC-MS/MS using Thermo Scientific Q Exactive Focus Orbitrap LC-MS/MS system. Purity of the final compounds was determined by LC-MS using the area percentage method on the UV trace recorded at a wavelength of 254 nm and found to be >95%.

General procedure A-1: Amide coupling to afford derivatives 3a, S3, S5a–S5q, S5t, S10a–S10d and S13a–S13c

The acid (1.2–2.0 eq) was dissolved in DCM. EDC·HCl (1.2–2.0 eq) was added, followed by the corresponding aniline (1.0 eq). The resultant mixture was stirred at room temperature, until the starting aniline was consumed. The obtained solution was washed with 1 M HCl and brine. The organic layer was dried over anhydrous sodium sulfate, filtered and concentrated under reduced pressure to afford the crude product. The obtained crude product was either used in the next step without further purification or purified using column chromatography.

General procedure A-2: Amide coupling to afford derivatives S5r–S5s and S5u

A mixture of 2-bromo-4-methylpentanoic acid (1.0 eq), thionyl chloride (10.0 eq) and DMF (5 drops) in THF was heated at 50 °C for 3 hours. The reaction mixture was cooled to room temperature, the solvent and the excess of thionyl chloride were removed under reduced pressure. The crude 2-bromo-4-methylpentanoyl chloride in THF was added at 0 °C under N_2 atmosphere to the corresponding aniline (1 eq). After 30 minutes at 0 °C, the ice bath was removed and the solution was warmed up and stirred at 50 °C for 2 hours. The reaction mixture was cooled to room temperature, the solvent was removed under reduced pressure. The reaction mixture was extracted with CH_2Cl_2 , the organic layer was dried over MgSO_4 , filtered and the solution was concentrated

under reduced pressure to afford the crude product. The obtained crude product was either used in the next step without further purification or purified using column chromatography.

General procedure B: Synthesis of imidazole and triazole derivatives 3k and 3m–3n

2-Bromo-4-methyl-*N*-(*p*-tolyl)pentanamide **S5a** (1.0 equiv.) was placed in a crimp vial and dissolved in acetone. Corresponding imidazole or triazole (1.1 equiv.) and K₂CO₃ (1.1 equiv.) were added and the mixture heated to 70 °C overnight (or otherwise specified). EtOAc was added, the organic layer washed with water and saturated aqueous NaCl solution, dried over anhydrous Na₂SO₄, filtered and concentrated under reduced pressure. The crude was purified by preparative HPLC.

General procedure C: Synthesis of diethyl phosphonate derivatives S7a–S7u, S11a–S11d and S14a–S14c

N-Aryl-2-halo-2-alkylacetamide derivative (1.0 eq) was suspended in triethyl phosphite (10 eq) and heated to 150 °C in a sealed tube for a total of 18 h (or otherwise specified). Most of unreacted triethyl phosphite was evaporated in vacuo and the resultant oil was purified by column chromatography.

General procedure D: Synthesis of phosphonic acid derivatives 4a–4ad

To a solution of diethyl phosphonate (1.0 eq) in dry DCM, bromotrimethylsilane (5.0–7.0 eq) was added dropwise over a period of 15 min. The reaction mixture was stirred at r.t. overnight (or otherwise specified). If no full conversion was achieved, the excess of bromotrimethylsilane (5.0 eq) was added next day. Then MeOH was added and stirred for 30 min at room temperature to cleave the previously formed TMS ester. Solvents were concentrated in vacuo and the resultant oil was purified by preparative HPLC.

Kinetic turbidimetric solubility. The desired compounds were sequentially diluted in DMSO in a 96-well plate. 1.5 μL of each well were transferred into another 96-well plate and mixed with 148.5 μL of PBS. Plates were shaken for 5 min at 600 rpm at room temperature (r.t.), and the absorbance at 620 nm was measured. Absorbance values were normalized by blank subtraction and plotted using GraphPad Prism 8.4.2 (GraphPad Software, San Diego, CA, USA). Solubility (S) was determined based on the First X value of AUC function using a threshold of 0.005.

Lipophilicity determination. LogD_{7.4} was analyzed using an HPLC–MS based method⁴⁶. The retention time of 12 compounds with known LogD_{7.4} was determined and plotted toward their LogD_{7.4}. Linear regression was used to determine the LogD_{7.4} of unknown compounds. Analysis was performed using a Dionex Ultimate 3000 HPLC system coupled to a TSQ Quantum Access

MAX (Thermo Fisher, Dreieich, Germany) with the following conditions: EC150/2 NUCLEODUR C18 Pyramid column, 5 μ M (Macherey Nagel, Düren, Germany); eluent A: 50 mM NH₄OAc pH 7.4, eluent B: acetonitrile, and flow: 0.6 mL/min. The gradient was set to 0–100% B from 0 to 2.5 min, 100% B from 2.5 to 3.0 min, 100–0% B from 3.0 to 3.2 min, and 0% B from 3.2–5.0.

Metabolic stability. For the evaluation of combined phase I and phase II metabolic stability, the compound (1 μ M) was incubated with 1 mg/mL pooled mouse liver S9 fraction (Xenotech, Kansas City, USA) or human liver S9 fraction (Corning, USA), 2 mM NADPH, 1 mM UDPGA, 10 mM MgCl₂, 5 mM GSH and 0.1 mM PAPS at 37 °C for 120 min. The metabolic stability of testosterone, verapamil and ketoconazole were determined in parallel to confirm the enzymatic activity of mouse S9 fractions, for human S9 testosterone, diclofenac and propranolol were used. The incubation was stopped after defined time points by precipitation of aliquots of S9 enzymes with 2 volumes of cold acetonitrile containing internal standard (150 nM diphenhydramine). Samples were stored on ice until the end of the incubation and precipitated protein was removed by centrifugation (15 min, 4 °C, 4,000 g). Concentration of the remaining test compound at the different time points was analyzed by HPLC-MS/MS (TSQ Quantum Access MAX, Thermo Fisher, Dreieich, Germany) and used to determine half-life ($t_{1/2}$) and intrinsic clearance (Cl_{int}). Species profiling was conducted as above using 0.5 mg/mL pooled mouse, rat or minipig liver microsomes (Xenotech, Kansas City, USA) with 2 mM NADPH and 10 mM MgCl₂ and testosterone, verapamil and ketoconazole as reference compounds.

Plasma stability. To determine stability in plasma, a similar setup as for the determination of metabolic stability was applied using pooled mouse/human/rat or minipig plasma (Neo Biotech, Nanterre, France). Samples were taken by mixing aliquots with 4 volumes of acetonitrile containing internal standard (125 nM diphenhydramine). The plasma stability of procain, propantheline and diltiazem were determined in parallel to confirm the enzymatic activity.

Calu-3 permeability. Compound permeability was assessed in vitro with Calu-3 HTB-55 cell line (ATCC). Cells were cultivated in Minimum Essential Medium supplemented with Earle's salts, L-glutamine, 10% FCS, 1% non-essential amino acids (NEAA) and 1mM sodium pyruvate. Passages between 35 and 55 were used, medium was changed every 2–3 days. For experiments, cells were harvested using trypsin/EDTA and 1x10⁵ cells seeded on Transwell® inserts 3460. Cells were grown in air-liquid interface beginning day 3 and used for transport studies on day 11–13. Transepithelial/transendothelial electrical resistance (TEER) values exceeded 300 Ω *cm² before

beginning transport studies. For experiments, Krebs-Ringer solution was used and cells were accommodated to the buffer for at least 1 h with no decrease in TEER. 200 μ L samples were taken in regular intervals from the apical side (time intervals 0, 15, 30, 60, 120, 180, 300 min) and replenished with fresh buffer. TEER was monitored during the experiment, and epithelial barriers were considered compromised if the TEER fell below 300 Ω *cm² during 5 h of experiment duration. A cassette of atenolol, ciprofloxacin and carbamazepine was used as control. Test compounds were applied individually or in cassettes including up to three compounds.

Before analysis, 40 μ L of sample was mixed with 80 μ L of ice-cold acetonitrile containing internal standard diphenhydramine (150 nM), and the compound concentration was analyzed with HPLC-ESI-MS/MS in SRM mode. Samples from the apical compartment taken at the beginning and end of the experiment were diluted 1:10 in KRB + 0.5% DMSO before mixing with acetonitrile.

Culturing of HepG2, A549 and HEK293 cells. The human hepatocellular carcinoma cell line HepG2, the lung adenocarcinoma cell line A549 and Human Embryonic (HEK) 293 cells were cultured in Dulbecco's Modified Eagle Medium (DMEM), containing 10% Fetal Bovine Serum (FBS) and 1% penicillin-streptomycin mixture. Cells were maintained according to standard cell culture procedures.

Cytotoxicity assay. An MTT-based assay was employed to evaluate the viability of HepG2, HEK293 and A549 cells after challenge with selected LasB inhibitors and performed as described previously⁴⁷.

Expression and purification of LasB and ColH-PD. LasB and ColH-PD were expressed and purified as described previously^{30,48}.

In vitro inhibition assays (LasB, ColH, MMPs, TACE, HDACs). All in vitro inhibition assays were performed as described previously^{30,49}. TACE and HDAC inhibitor screening kits were purchased from Sigma-Aldrich (Saint Louis, MO). MMPs along with the SensoLyte 520 Generic MMP Activity Kit Fluorimetric were purchased from AnaSpec (Fremont, CA, USA), and the fluorometric cyclooxygenase 1 (COX1) inhibitor assay kit was purchased from Abcam (Cambridge, UK). The assays were performed according to the guidelines of the respective manufacturer. Fluorescence signals were measured using a CLARIOstar plate reader (BMG Labtech, Ortenberg, Germany). Pulmonary surfactant (poractant alfa), which is an extract of natural porcine lung surfactant, was purchased from Creative BioMart (Shirley, NY, USA).

PA14 csn production. The csn of wt PA14 and Δ lasB PA14 was produced as we previously reported³¹.

Validation of the effect of LasB inhibitors on A549 cells *in vitro*. The experiment was performed as described previously³¹. The Picrosirius red assay was performed by washing the csn-challenged cells (\pm inhibitor) 3x with PBS followed by an incubation with Bouin solution (Sigma) at RT for 20 min. The cells were incubated with 0.1% Picrosirius red dye (ab150681) at RT for 2 h. Then, they were washed once with 0.01 N HCl, and the matrix was dissolved in 0.01 N NaOH. The absorption was measured at 570 nm using a PHERAstar plate reader (BMG Labtech). By dividing the absorbance of each sample by the absorbance of the healthy sample, the relative collagen quantity was determined. For each condition, the experiment was performed three times. To determine the rescue of A549 cells treated with 5% wt PA14 csn using our compounds, the LasB inhibitors were used at 2, 0.5, 0.1 and 0.05 μ M. The compounds were incubated in F12K medium, then deposited on the cells for 24 h. Cell detachment was then evaluated, and a Trypan Blue cell count was determined. Based on these results, IC₅₀ values were determined.

To investigate the effect of **4a** and **4b** on the viability of A549 cells after challenge with culture supernatant (csn) of *Pseudomonas aeruginosa* PAO1 (DSM 22644, ATCC 15692), 2.5*10³ cells/well were seeded into a flat bottom 96-well plate (Corning™ Costar™) and incubated at 37 °C + 5% CO₂ for 24 h. On the following day, several concentrations of the compounds **4a** and **4b** were tested against 10% (v/v) *P. aeruginosa* PAO1 csn diluted in DMEM starting from 10 μ M and 20 μ M, respectively. Compound was initially dissolved in DMSO, and a low final assay concentration of 0.5% (v/v) was applied to minimize the proteolytic effect of DMSO on the bacterial culture supernatant. In addition, cells were challenged with 10% (v/v) of Δ lasB PAO1 to confirm the cytotoxic effect derived from LasB, and DMEM was included as a control without any treatment. Plates were incubated at 37 °C + 5% CO₂ for 24 h prior to the MTT assay (described above). Finally, data were statistically analyzed and graphically displayed using GraphPad Prism 9.

Comparison of the activity of LasB in culture supernatants of PAO1 and PA14 using a FRET-based proteolytic assay. Bacterial culture supernatant of *P. aeruginosa* strains PAO1 and PA14 was prepared from overnight cultures in lysogeny broth medium (LB). The cultures were centrifuged after approx. 18 hours and filtered using 0.2 μ m non-pyrogenic sterile filters. The fluorogenic substrate 2-Aminobenzoyl-Ala-Gly-Leu-Ala-4-Nitrobenzylamide was supplied from Peptides International (Louisville, KY, USA) for use in this study. Fluorescence intensity was measured for 30 min at 37 °C using a CLARIOstar microplate reader (BMG Labtech, Ortenberg, Germany), with excitation and emission wavelengths of 340 \pm 15 nm and 415 \pm 20 nm,

respectively, in black 384-well microtiter plates (Greiner Bio-One, Kremsmünster, Austria). The experiment was carried out in a final volume of 50 μ L, containing assay buffer (50 mM Tris, pH 7.2, 2.5 mM CaCl₂, 0.075% Pluronic F-127, 5% DMSO), PA14 and PAO1 supernatant at a final dilution factor of 5-5, and the substrate at a final concentration of 150 μ M. Each sample was included in the multi-well plate in duplicates, and controls without supernatant were included for blank correction. After blank subtraction, the FRET signal of samples containing supernatant at different time points (every two minutes) was plotted using GraphPad Prism 9 (Graph Pad Software, San Diego, CA, USA).

Lung organoid assay. Primary basal cells were isolated as described previously⁵⁰. The protocol was approved by the institutional review board of the Landesärztekammer of the State of Saarland. Informed consent was obtained from the patients. Basal cells were differentiated to 3D bronchospheres as described before⁴². In brief, 80 μ L of passage 1 basal cells (3×10^4 cells per mL differentiation media) were plated in each well of a 96-well plate containing 40 μ L of a 25% Matrigel solution (Corning, USA). 120 μ L differentiation media were added to the top every 4 days. At day 21, 120 μ L media were removed from the top, and 120 μ L differentiation media containing indicated concentrations of inhibitors were added. After 2 h, 120 μ L media were removed, and 120 μ L differentiation media with indicated concentrations of inhibitors with/without PA14 supernatants were added. After 48 h, 120 μ L media were removed, and the MTT assay was performed following the manufacturer's instructions (MTT Cell Viability Assay Kit, biotium USA).

***G. mellonella* infection model.** The infection model was performed as described before with minor modifications (each larva was injected with 4 bacteria)³⁰. Injections were carried out using an LA120 syringe pump (Landgraf Laborsysteme, Langenhagen, Germany) equipped with 1 mL Injekt-F tuberculin syringes (B. Braun, Melsungen, Germany) and Sterican 0.30 \times 12 mm², 30 G \times 1.5 needles (B. Braun). Larvae were incubated at 37 °C for 3 days and inspected twice daily. The total larvae used in all three experiments were 30 larvae per group. When the larvae became black and did not move when simulated with a tweezer, they were deemed dead.

Zebrafish embryo toxicity. The experiment was performed according to a procedure described in the literature⁵¹ with minor modifications using zebrafish embryos of the AB wild-type line at 1 day post fertilization (dpf). A detailed protocol has been given in our recent publication³³.

PK studies in mice.

Mice. For PK experiments, outbred male CD-1 mice (Charles River, Germany), 4 weeks old, were used. The animal studies were conducted in accordance with the recommendations of the European Community (Directive 86/609/EEC, 24 November 1986). All animal procedures were performed in strict accordance with the German regulations of the Society for Laboratory Animal Science (GV- SOLAS) and the European Health Law of the Federation of Laboratory Animal Science Associations (FELASA). Animals were excluded from further analysis, if sacrifice was necessary according to the human endpoints established by the ethical board. All experiments were approved by the ethical board of the Niedersächsisches Landesamt für Verbraucherschutz und Lebensmittelsicherheit, Oldenburg, Germany.

PK studies. Compounds **3g**, **3i**, **3l**, **4a** and **4b** were dissolved in 2 % DMSO, 1 % Tyloxapol and 97 % PBS. The compounds were administered intratracheally (IT) at 0.25 mg/kg per compound as cassette. Up to 5 compounds were dosed per cassette. Before administration, mice were anesthetized using ketamine 100 mg/kg and xylazine 10 mg/kg intraperitoneally. Mice (n=3 per time point) were euthanized at t= 0.5, 2 and 5 h post administration. **4b** was administered at 10 mg/kg using a Kent Scientific Aeroneb® nebulizer. Mice (n=3 per time point) were euthanized at t= 0.25, 0.5, 1, 2, 4, 8 and 24 h post administration. Blood was collected from the heart. Whole blood was collected into Eppendorf tubes coated with 0.5 M EDTA and immediately spun down at 13,000 rpm for 10 min at 4 °C. The plasma was transferred into a new Eppendorf tube and then stored at –80 °C until analysis. Then, a bronchoalveolar lavage was conducted using isotonic sodium chloride solution. Lung, kidneys, and liver were aseptically removed and homogenized using a Polytron tissue homogenizer (Kinematica) in isotonic sodium chloride solution. Organ samples were aliquoted into Eppendorf tubes and stored at –80 °C until analysis. Moreover, spontaneous urine was also collected. *Bioanalytical sample preparation.* All PK plasma samples were analyzed via HPLC-MS/MS using an Agilent 1290 Infinity II HPLC system and coupled to an AB Sciex QTrap6500+ mass spectrometer. First, a calibration curve was prepared by spiking different concentrations of **3g**, **3i**, **3l**, **4a** and **4b** into the respective matrix (mouse plasma (pooled, from CD-1 mice) for plasma samples, isotonic sodium chloride solution for BALF samples, lung tissue for lung samples, kidney tissue for kidney samples, liver tissue for liver samples and urine for urine samples). Caffeine was used as an internal standard. In addition, quality control samples (QCs) were prepared for **3g**, **3i**, **3l**, **4a** and **4b** with the respective matrix. The following extraction procedure was used: 7.5 µL of a plasma sample (calibration samples, QCs or PK samples) was

5 extracted with 37.5 μ L of methanol containing 12.5 ng/mL of caffeine as internal standard for 5 min at 2,000 rpm on an Eppendorf MixMate® vortex mixer. 10 μ L of a urine sample (calibration samples, QCs or PK samples) was extracted with 40 μ L of methanol containing 12.5 ng/mL of caffeine as internal standard for 5 min at 2000 rpm on an Eppendorf MixMate® vortex mixer. Then samples (plasma and urine) were spun down at 13,000 rpm for 5 min. Supernatants were transferred to standard HPLC-glass vials. 50 μ L of a BALF / lung tissue / kidney tissue or liver tissue sample (calibration samples, QCs or PK samples) were extracted with 50 μ L of methanol and 1 μ L caffeine (concentration 1 μ g/mL in methanol) for 5 min at 800 rpm on an Eppendorf MixMate® vortex mixer. Then samples (BALF, liver, kidney, lung) were spun down at 4,000 rpm for 40 min at 4 °C. Supernatants were transferred to 96well V-bottom plates (Greiner). HPLC conditions were as follows: column: Agilent Zorbax Eclipse Plus C18, 50x2.1 mm, 1.8 μ m; temperature: 30 °C; injection volume: 5 μ L; flow rate: 700 μ L/min; solvent A: water + 0.1% formic acid; solvent B: acetonitrile + 0.1% formic acid; gradient: 99% A at 0 min and until 1 min, 99% – 0% A from 1.0 min to 2.2 min, 0% A until 4 min. Mass spectrometric conditions were as follows: Scan type: MRM, negative and positive mode; Q1 and Q3 masses for caffeine, urea, **3g**, **3i**, **3l**, **4a** and **4b** can be found in Table S14. Urea was used to enable calculation of epithelial lining fluid (ELF) concentrations. Peak areas of each sample and of the corresponding internal standard were analyzed using MultiQuant 3.0 software (AB Sciex). Peak areas of the respective sample were normalized to the internal standard peak area. The MS/MS pairs used for quantification are marked with a ‘Q’ in the table, the other MS/MS pairs for the respective compound were used for qualification. Peaks of PK samples were quantified using the calibration curve. The accuracy of the calibration curve was determined using QCs independently prepared on different days. PK parameters were determined using a non-compartmental analysis with PKSolver⁵². ELF concentrations were calculated using the following formula⁵³:

$$(1) V_{ELF} = V_{BALF} \times \frac{Urea_{BALF}}{Urea_{plasma}}$$
$$(2) c_{ELF} = c_{BALF} \times \frac{V_{BALF}}{V_{ELF}}$$

Pharmacodynamic (PD) study with 4b and *P. aeruginosa*. For the therapeutic neutropenic pneumonia model, female CD-1 mice, 8-weeks-old, (Charles River, Germany) were rendered neutropenic by administration of 150 mg/kg and 100 mg/kg cyclophosphamide i.p. on day –4 and –1, respectively. The inoculum was prepared as follows: on day -1 the *P. aeruginosa* strain DSM-1117 (=ATCC 27853) was streaked out onto a blood agar plate and incubated at 37 °C. Then one

single colony was inoculated into LB medium (diluted 1:6 in water) containing 0.01% mucin and incubated at 120 rpm and 37 °C. On day 0 bacteria were centrifuged for 15 min at 4,000 rpm and washed twice in 0.9 % NaCl-solution. Then they were adjusted to an OD of 10. For infection with *P. aeruginosa* an inoculum of 1.2×10^9 cfu/mL was used. At d0 mice were infected by nebulization using an Aeroneb® nebulizer (Kent Scientific) of 20 μ L 1.2×10^9 CFU/ml *P. aeruginosa* DSM-1117. To control bacterial burden after nebulization, two animals were used as inoculum control group. The following groups were used: (1) vehicle control group, (2) levofloxacin group with 25 mg/kg IP QD (t= 2 h p.i.); (3) **4b** group with 10 mg/kg inhaled (t= 2, 6 and 10 h p.i.); (4) **4b** 10 mg/kg inhaled TID (t= 2, 6 and 10 h) combined with levofloxacin at 25 mg/kg IP QD (t= 2 h p.i.). After 24 h p.i., mice were euthanized for terminal analysis. After isolation of blood, lung was removed, weighed, and homogenized in 3 mL 0.9% NaCl. For determination of CFUs, suspensions of homogenized organs were serially diluted, plated on agar plates and incubated overnight at 37 °C. CFUs were determined by manual counting.

LC-MS/MS assay for determination of LasB in whole blood samples. All samples were analyzed via HPLC-MS/MS using an Agilent 1290 Infinity II HPLC system and coupled to an AB Sciex QTrap7500 mass spectrometer. Blood samples from the PD study with **4b** and *P. aeruginosa* were extracted as follows: 50 μ L of a blood sample was extracted with 50 μ L of acetonitrile for 5 min at 2,000 rpm on an Eppendorf MixMate® vortex mixer. Then samples were spun down at 13,000 rpm for 5 min. Supernatants were transferred to standard HPLC-glass vials. HPLC conditions were as follows: column: Agilent Zorbax Eclipse Plus C18, 50x2.1 mm, 1.8 μ m; temperature: 30 °C; injection volume: 5 μ L; flow rate: 700 μ L/min; solvent A: water + 0.1% formic acid; solvent B: acetonitrile + 0.1% formic acid; gradient: 99% A at 0 min and until 1 min, 99% – 0% A from 1.0 min to 3 min, 0% A until 4.7 min. Mass spectrometric conditions were as follows: Scan type: MRM, positive mode; Source temperature: 500 °C; Spray voltage: 2000 V; EP in volts was set to 10 for every transition. Likewise, CXP in volts was set to 17.5. Dwell time was 3 msec for every transition.

Bacterial growth inhibition assay. Assays regarding the determination of the MIC were performed as described recently for *P. aeruginosa* PA14⁵⁴.

X-ray crystallography. LasB was expressed and purified as described previously³⁰. The protein was concentrated to 12 mg/mL and mixed with compound **4b** at a final concentration of 1 mM. Complex crystals were obtained in 0.1 M Tris-Cl pH 8.5, and 1.6 ammonium sulfate. Crystals were cryoprotected in glycerol, and diffraction data was collected from single crystals at 100 K at

beamline P11 at Petra III (DESY) at a wavelength of 0.967 Å⁵⁵. Data were processed using Xia2 or XDS, and the structure solved using PHASER Molecular Replacement with *P. aeruginosa* elastase (PDB ID 1EZM) as a search model^{56,57,58,59}. The models were manually rebuilt with COOT and refined using PHENIX and Refmac5^{59,60,61}.

5

References

- ¹ WHO Antibiotic resistance - Fact sheets, 31 July 2020, <https://www.who.int/news-room/fact-sheets/detail/antibiotic-resistance>
- ² Ventola, C. L. The Antibiotic Resistance Crisis, Part 1: Causes and Threats. *P & T* **40**, 277–283 (2015).
- ³ Antimicrobial Resistance Collaborators, Global burden of bacterial antimicrobial resistance in 2019: a systematic analysis. *Lancet* **399**, 629–655 (2022).
- ⁴ GBD 2019 Antimicrobial Resistance Collaborators, Global mortality associated with 33 bacterial pathogens in 2019: a systematic analysis for the Global Burden of Disease Study 2019. *Lancet* **400**, 2221–2248 (2022).
- ⁵ Bassetti, M., Vena, A., Croxatto, A., Righi, E., Guery, B. How to manage *Pseudomonas aeruginosa* infections. *Drugs Context* 7:212527 (2018).
- ⁶ WHO priority pathogens list, <https://www.who.int/news/item/27-02-2017-who-publishes-list-of-bacteria-for-which-new-antibiotics-are-urgently-needed>
- ⁷ Malhotra, S., Hayes, D., Wozniak, D. J. Cystic Fibrosis and *Pseudomonas aeruginosa*: the Host-Microbe Interface. *Clin. Microbiol. Rev.* **32**, e00138-18 (2019).
- ⁸ Woo, T. E., Duong, J., Jervis, N. M., Rabin, H. R., Parkins, M. D., Storey, D. G. Virulence adaptations of *Pseudomonas aeruginosa* isolated from patients with non-cystic fibrosis bronchiectasis. *Microbiology (Reading)* **162**, 2126–2135 (2016).
- ⁹ Spellberg, B., Talbot, G. Recommended Design Features of Future Clinical Trials of Antibacterial Agents for Hospital-Acquired Bacterial Pneumonia and Ventilator-Associated Bacterial Pneumonia. *Clin Infect Dis* **51** (suppl. 1), 150–170 (2010).
- ¹⁰ Koenig, S. M., Truwit, J. D. Ventilator-associated pneumonia: diagnosis, treatment, and prevention. *Clin Microbiol Rev.* **19**, 637–657 (2006).

-
- ¹¹ Lamas Ferreira, J. L., Álvarez Otero, J., González González, L., Novoa Lamazares, L., Arca Blanco, A., Bermúdez Sanjurjo, J. R., Rodríguez Conde, I., Fernández Soneira, M., de la Fuente Aguado, J. *Pseudomonas aeruginosa* urinary tract infections in hospitalized patients: Mortality and prognostic factors. *PLoS One*. **12**, e0178178 (2017).
- ¹² Hilliam, Y., Kaye, S., Winstanley, C. *Pseudomonas aeruginosa* and microbial keratitis. *J Med Microbiol*. **69**, 3–13 (2020).
- ¹³ Kirketerp-Møller, K., Jensen, P. Ø., Fazli, M., Madsen, K. G., Pedersen, J., Moser, C., Tolker-Nielsen, T., Høiby, N., Givskov, M., Bjarnsholt, T. Distribution, Organization, and Ecology of Bacteria in Chronic Wounds. *J Clin Microbiol*. **46**, 2717–2722 (2008).
- ¹⁴ Walesch, S., Birkelbach, J., Jézéquel, G., Haeckl, F. P. J., Hegemann, J. D., Hesterkamp, T., Hirsch, A. K. H., Hammann, P., Müller, R. Fighting antibiotic resistance—strategies and (pre)clinical developments to find new antibacterials. *EMBO Reports* **24**, e56033 (2023).
- ¹⁵ Wagner, S., Sommer, R., Hinsberger, S., Lu, C., Hartmann, R. W., Empting, M., Titz, A. Novel Strategies for the Treatment of *Pseudomonas aeruginosa* Infections. *J. Med. Chem.* **59**, 5929–5969 (2016).
- ¹⁶ Calvert, M. B., Jumde, V. R., Titz, A. Pathoblockers or antivirulence drugs as a new option for the treatment of bacterial infections. *Beilstein J. Org. Chem.* **14**, 2607–2617 (2018).
- ¹⁷ Rezzoagli, C., Archetti, M., Mignot, I., Baumgartner, M., Kümmerli, R. Combining antibiotics with antivirulence compounds can have synergistic effects and reverse selection for antibiotic resistance in *Pseudomonas aeruginosa*. *PLOS Biol* **18**, e3000805 (2020).
- ¹⁸ Khalifa, A. B. H., Moissenet, D., Thien, H. V., Khedher, M. Virulence factors in *Pseudomonas aeruginosa*: mechanisms and modes of regulation. *Ann Biol Clin.* **69**, 393–403 (2011).
- ¹⁹ Wretling, B., Pavlovskis, O. R. *Pseudomonas aeruginosa* elastase and its role in pseudomonas infections. *Rev Infect Dis.* **5** (suppl. 5), 998–1004 (1983).
- ²⁰ Everett, M. J., Davies, D. T. *Pseudomonas aeruginosa* elastase (LasB) as a therapeutic target. *Drug Discov Today.* **26**, 2108–2123 (2021).
- ²¹ Zupetic, J., Peñaloza, H. F., Bain, W., Hulver, M., Mettus, R., Jorth, P., Doi, Y., Bomberger, J., Pilewski, J., Nouriaie, M., Lee, J. S. Elastase Activity From *Pseudomonas aeruginosa* Respiratory Isolates and ICU Mortality. *Chest.* **160**, 1624–1633 (2021).

-
- ²² Galdino, A. C. M., Viganor, L., de Castro, A. A., da Cunha, E. F. F., Mello, T. P., Mattos, L. M., Pereira, M. D., Hunt, M. C., O'Shaughnessy, M., Howe, O., Devereux, M., McCann, M., Ramalho, T. C., Branquinha, M. H., Santos, A. L. S. Disarming *Pseudomonas aeruginosa* Virulence by the Inhibitory Action of 1,10-Phenanthroline-5,6-Dione-Based Compounds: Elastase B (LasB) as a Chemotherapeutic Target. *Front. Microbiol.* **10**, 1701 (2019).
- ²³ Cathcart, G. R. A., Quinn, D., Greer, B., Harriott, P., Lynas, J. F., Gilmore, B. F., Walker, B. Novel Inhibitors of the *Pseudomonas aeruginosa* Virulence Factor LasB: a Potential Therapeutic Approach for the Attenuation of Virulence Mechanisms in Pseudomonal Infection. *Antimicrob Agents Chemother.* **55**, 2670–2678 (2011).
- ²⁴ Zhu, J., Cai, X., Harris, T. L., Gooyit, M., Wood, M., Lardy, M., Janda, K. D. Disarming *Pseudomonas aeruginosa* virulence factor LasB by leveraging a *Caenorhabditis elegans* infection model. *Chem. Biol.* **22**, 483–491 (2015).
- ²⁵ Grobelny, D., Poncz, L., Galardy, R. E. Inhibition of human skin fibroblast collagenase, thermolysin, and *Pseudomonas aeruginosa* elastase by peptide hydroxamic acids. *Biochemistry.* **31**, 7152–7154 (1992).
- ²⁶ Everett, M. J., Davies, D. T., Leiris, S., Sprynski, N., Llanos, A., Castandet, J. M., Lozano, C., LaRock, C. N., LaRock, D. L., Corsica, G., Docquier, J-D., Pallin, T. D., Cridland, A., Blench, T., Zalacain, M., Lemonnier, M. Chemical Optimization of Selective *Pseudomonas aeruginosa* LasB Elastase Inhibitors and Their Impact on LasB-Mediated Activation of IL-1 β in Cellular and Animal Infection Models. *ACS Infect. Dis.* **9**, 270–282 (2023).
- ²⁷ Fullagar, J. L., Garner, A. L., Struss, A. K., Day, J. A., Martin, D. P., Yu, J., Cai, X., Janda, K. D., Cohen, S. M. Antagonism of a Zinc Metalloprotease Using a Unique Metal-Chelating Scaffold: Tropolones as Inhibitors of *P. aeruginosa* Elastase. *Chem Commun (Camb).* **49**, 3197–3199 (2013).
- ²⁸ Garner, A. L., Struss, A. K., Fullagar, J. L., Agrawal, A., Moreno, A. Y., Cohen, S. M., Janda, K. D. 3-Hydroxy-1-alkyl-2-methylpyridine-4(1H)-thiones: Inhibition of the *Pseudomonas aeruginosa* Virulence Factor LasB. *ACS Med Chem Lett.* **3**, 668–672 (2012).
- ²⁹ Voos, K., Yahiaoui, S., Konstantinović, J., Schönauer, E., Alhayek, A., Sikandar, A., Chaib, K. S., Ramspoth, T., Rox, K., Hauptenthal, J., Köhnke, J., Brandstetter, H., Ducho, C., Hirsch, A. K. H. *N*-Aryl-2-iso-butylmercaptoacetamides: the discovery of highly potent and selective inhibitors

of *Pseudomonas aeruginosa* virulence factor LasB and *Clostridium histolyticum* virulence factor ColH. chemRxiv [Preprint] (2022). <https://doi.org/10.26434/chemrxiv-2022-fjrqr>.

³⁰ Kany, A. M., Sikandar, A., Haupenthal, J., Yahiaoui, S., Maurer, C. K., Proschak, E., Köhnke, J., Hartmann, R. W. Binding Mode Characterization and Early in Vivo Evaluation of Fragment-Like Thiols as Inhibitors of the Virulence Factor LasB from *Pseudomonas aeruginosa*. *ACS Infect. Dis.* **4**, 988–997 (2018).

³¹ Kaya, C., Walter, I., Yahiaoui, S., Sikandar, A., Alhayek, A., Konstantinović, J., Kany, A. M., Haupenthal, J., Köhnke, J., Hartmann, R. W., Hirsch, A. K. H. Substrate-Inspired Fragment Merging and Growing Affords Efficacious LasB Inhibitors. *Angew. Chem. Int. Ed.* **61**, e202112295 (2022).

³² Kaya, C., Walter, I., Alhayek, A., Shafiei, R., Jézéquel, G., Andreas, A., Konstantinović, J., Schönauer, E., Sikandar, A., Haupenthal, J., Müller, R., Brandstetter, H., Hartmann, R. W., Hirsch, A. K. H. Structure-Based Design of α -Substituted Mercaptoacetamides as Inhibitors of the Virulence Factor LasB from *Pseudomonas aeruginosa*. *ACS Infect. Dis.* **8**, 1010–1021 (2022).

³³ Konstantinović, J., Yahiaoui, S., Alhayek, A., Haupenthal, J., Schönauer, E., Andreas, A., Kany, A. M., Müller, R., Koehnke, J., Berger, F. K., Bischoff, M., Hartmann, R. W., Brandstetter, H., Hirsch, A. K. H. *N*-Aryl-3-mercaptosuccinimides as Antivirulence Agents Targeting *Pseudomonas aeruginosa* Elastase and *Clostridium* Collagenases. *J. Med. Chem.* **63**, 8359–8368 (2020).

³⁴ Voos, K., Schönauer, E., Alhayek, A., Haupenthal, J., Andreas, A., Müller, R., Hartmann, R. W., Brandstetter, H., Hirsch, A. K. H., Ducho, C. Phosphonate as a Stable Zinc-Binding Group for “Pathoblocker” Inhibitors of Clostridial Collagenase H (ColH). *ChemMedChem* **16**, 1257–1267 (2021).

³⁵ Nishino, N., Powers, J. C. *Pseudomonas aeruginosa* elastase. Development of a new substrate, inhibitors, and an affinity ligand. *J. Biol. Chem.* **255**, 3482–3486 (1980).

³⁶ Silverman, J. A., Mortin, L. I., Vanpraagh, A. D., Li, T., Alder, J. Inhibition of daptomycin by pulmonary surfactant: in vitro modeling and clinical impact. *J Infect Dis.* **191**, 2149–2152 (2005).

³⁷ Fluorescence Microscopy of Living Cells in Culture Part B. Quantitative Fluorescence Microscopy—Imaging and Spectroscopy. *Methods Cell Biol* **30**, 1–498 (1989).

-
- ³⁸ Borges, L. F., Taboga, S. R., Gutierrez, P. S. Simultaneous observation of collagen and elastin in normal and pathological tissues: analysis of Sirius-red-stained sections by fluorescence microscopy. *Cell Tissue Res.* **320**, 551–552 (2005).
- ³⁹ Alhayek, A., Abdelsamie, A. S., Schönauer, E., Camberlein, V., Hutterer, E., Posselt, G., Serwanja, J., Blöchl, C., Huber, C. G., Hauptenthal, J., Brandstetter, H., Wessler, S., Hirsch, A. K. H. Discovery and Characterization of Synthesized and FDA-Approved Inhibitors of Clostridial and Bacillary Collagenases. *J. Med. Chem.* **65**, 12933–12955 (2022).
- ⁴⁰ Kong, J., Wen, S., Cao, W., Yue, P., Xu, X., Zhang, Y., Luo, L., Chen, T., Li, L., Wang, F., Tao, J., Zhou, G., Luo, S., Liu, A., Bao, F. Lung organoids, useful tools for investigating epithelial repair after lung injury. *Stem Cell Res. Ther.* **12**, 95 (2021).
- ⁴¹ Cunniff, B., Druso, J. E., van der Velden, J. L. Lung organoids: advances in generation and 3D-visualization. *Histochem. Cell Biol.* **155**, 301–308 (2021).
- ⁴² Sprott, R. F., Ritzmann, F., Langer, F., Yao, Y., Herr, C., Kohl, Y., Tschernig, T., Bals, R., Beisswenger, C. Flagellin shifts 3D bronchospheres towards mucus hyperproduction. *Respir Res* **21**, 222 (2020).
- ⁴³ Tsai, C. JY., Loh, J. M. S., Proft, T. *Galleria mellonella* infection models for the study of bacterial diseases and for antimicrobial drug testing, *Virulence* **7**, 214-229 (2016).
- ⁴⁴ Taccetti, G., Francalanci, M., Pizzamiglio, G., Messori, B., Carnovale, V., Cimino, G., Cipolli, M. Cystic Fibrosis: Recent Insights into Inhaled Antibiotic Treatment and Future Perspectives. *Antibiotics* **10**, 338 (2021).
- ⁴⁵ Xu, M. J., Dai, B. Inhaled antibiotics therapy for stable non-cystic fibrosis bronchiectasis: a meta-analysis. *Ther Adv Respir Dis.* **14**, 1753466620936866 (2020).
- ⁴⁶ Klingler, F-M., Wichelhaus, T. A., Frank, D., Cuesta-Bernal, J., El-Delik, J., Müller, H. F., Sjuts, H., Göttig, S., Koenigs, A., Pos, K. M., Pogoryelov, D., Proschak, E. Approved Drugs Containing Thiols as Inhibitors of Metallo- β -lactamases: Strategy To Combat Multidrug-Resistant Bacteria. *J. Med. Chem.* **58**, 3626–3630 (2015).
- ⁴⁷ Hauptenthal, J., Baehr, C., Zeuzem, S., Piiper, A. RNase A-like enzymes in serum inhibit the anti-neoplastic activity of siRNA targeting polo-like kinase 1. *Int. J. Cancer* **121**, 206–210 (2007).

-
- ⁴⁸ Eckhard, U., Schönauer, E., Brandstetter, H. Structural Basis for Activity Regulation and Substrate Preference of Clostridial Collagenases G, H, and T. *J. Biol. Chem.* **288**, 20184–20194 (2013).
- ⁴⁹ Schönauer, E., Kany, A. M., Haupenthal, J., Hüsecken, K., Hoppe, I. J., Voos, K., Yahiaoui, S., Elsässer, B., Ducho, C., Brandstetter, H., Hartmann, R. W. Discovery of a Potent Inhibitor Class with High Selectivity toward Clostridial Collagenases. *J. Am. Chem. Soc.* **139**, 12696–12703 (2017).
- ⁵⁰ Bals, R., Beisswenger, C., Blouquit, S., Chinet, T. Isolation and air–liquid interface culture of human large airway and bronchiolar epithelial cells. *J Cyst Fibros.* **3** (suppl 2), 49–51 (2004).
- ⁵¹ Maes, J., Verlooy, L., Buenafe, O. E., de Witte, P. A. M., Esguerra, C. V., Crawford, A. D. Evaluation of 14 Organic Solvents and Carriers for Screening Applications in Zebrafish Embryos and Larvae. *PLoS One* **7**, e43850 (2012).
- ⁵² Zhang, Y., Huo, M., Zhou, J., Xie, S. PKSolver: An add-in program for pharmacokinetic and pharmacodynamic data analysis in Microsoft Excel. *Comput. Methods Programs Biomed.* **99**, 306–314 (2010).
- ⁵³ Kiem, S., Schentag, J. J. Interpretation of antibiotic concentration ratios measured in epithelial lining fluid. *Antimicrob. Agents Chemother.* **52**, 24–36 (2008).
- ⁵⁴ Elgaher, W., Fruth, M., Groh, M., Haupenthal, J., Hartmann, R. W. Expanding the scaffold for bacterial RNA polymerase inhibitors: design, synthesis and structure–activity relationships of ureido-heterocyclic-carboxylic acids. *RSC Adv.* **4**, 2177–2194 (2014).
- ⁵⁵ Burkhardt, A., Pakendorf, T., Reime, B., Meyer, J., Fischer, P., Stübe, N., Panneerselvam, S., Lorbeer, O., Stachnik, K., Warmer, M., Rödig, P., Göries, D., Meents, A. Status of the crystallography beamlines at PETRA III. *Eur. Phys. J. Plus* **131**, 56 (2016).
- ⁵⁶ Winter, G. Xia2: An Expert System for Macromolecular Crystallography Data Reduction. *J. Appl. Crystallogr.* **43**, 186–190 (2010).
- ⁵⁷ Kabsch, W. XDS. *Acta Crystallogr. Sect. D Biol. Crystallogr.* **66**, 125–132 (2010).
- ⁵⁸ McCoy, A. J., Grosse-Kunstleve, R. W., Adams, P. D., Winn, M. D., Storoni, L. C., Read, R. J. Phaser Crystallographic Software. *J. Appl. Crystallogr.* **40**, 658–674 (2007).
- ⁵⁹ Emsley, P., Lohkamp, B., Scott, W. G., Cowtan, K. Features and Development of Coot. *Acta Crystallogr. D. Biol. Crystallogr.* **66**, 486–501 (2010).

⁶⁰ Adams, P. D., Afonine, P. V., Bunkóczi, G., Chen, V. B., Davis, I. W., Echols, N., Headd, J. J., Hung, L.-W., Kapral, G. J., Grosse-Kunstleve, R. W., McCoy, A. J., Moriarty, N. W., Oeffner, R., Read, R. J., Richardson, D. C., Richardson, J. S., Terwilliger, T. C., Zwart, P. H. PHENIX: A Comprehensive Python-Based System for Macromolecular Structure Solution. *Acta Crystallogr. D. Biol. Crystallogr.* **66**, 213–221 (2010).

⁶¹ Skubák, P., Murshudov, G. N., Pannu, N. S. Direct Incorporation of Experimental Phase Information in Model Refinement. *Acta Crystallogr. Sect. D* **60**, 2196–2201 (2004).

Acknowledgments: The authors thank S. Wolter, S. Speicher, J. Jung, S. Amann, P. Paul and T. Trampert for excellent technical support and V. Camberlein and C. Schütz for providing important intermediates. Moreover, the authors thank A. Ahlers, J. Schreiber, K.V. Sander and J. Wolf for excellent technical assistance. The authors acknowledge DESY (Hamburg, Germany), a member of the Helmholtz Association HGF, for the provision of experimental facilities. Parts of this research was carried out at PETRAIII, and we would like to thank Dr. Johanna Hakanpää for assistance in using photon beamline. Beamtime was allocated for proposal (Xh-20010236).

Funding:

CARB-X funding ID 05CARB-X0891 (AKHH)

European Research Council, ERC starting grant 757913 (AKHH)

Helmholtz-Association's Initiative and Networking Fund (AKHH)

Austrian Science Fund (FWF), P 31843 (ES)

German Federal Ministry of Education and Research (BMBF), call "Alternative methods to animal experiments" (project 3-REPLACE, 16LW0140K) (CB, RM)

Alexander von Humboldt Foundation (JK)

Author contributions:

Design of the study: JK, AMK, RWH, KR, JH, AKHH

Project management: JH, AKHH

Design and synthesis of inhibitors: JK, ASA, KV, CD

Evaluation of LasB activity: JK

ADMET profiling: AMK

Calu-3 assay: BL, CML

Experiments on A549 cells: AIA, RS

Galleria mellonella experiment: AIA

Lung organoid assay: CB, RB, YY

Cytotoxicity and selectivity profile: JH

Zebrafish embryo toxicity: AnA, RM

Evaluation of ColH activity: ES, HB

PK and PD studies and LC-MS/MS assays on LasB: KR

X-Ray: AS, RM

Writing – original draft: JK

Writing – review & editing: JK, AMK, JH, KR, AKHH, with a contribution of all authors

All authors discussed the results and commented on the manuscript.

Competing interests: The authors declare the following competing financial interest(s): JK, KV, ASA, AMK, JH, CD, AKHH and RWH are co-inventors on a international patent application (PCT/EP2021/073381) that incorporates methods outlined in this manuscript.

Data and materials availability: All data are available in the main text or the supplementary information.

Materials and Correspondence: Please address all correspondence and material requests to Anna K.H. Hirsch (Email: anna.hirsch@helmholtz-hips.de)